crystals

MDPI

*Article*

# Structural Characterization and Pharmaceutical Evaluation of Telmisartan Hydrochloride Salts

**Yuda Prasetya Nugraha [1,*], I Gusti Ayu Nadia Prasta Unique [1], Tatsuki Miyake [2], Ridha Rahmah [1], Indra Indra [1], Sundani Nurono Soewandhi [1] and Hidehiro Uekusa [2,*]**

[1] Department of Pharmaceutics, School of Pharmacy, Bandung Institute of Technology, Bandung 40132, Indonesia
[2] Department of Chemistry, School of Science, Tokyo Institute of Technology, Ookayama 2-12-1, Meguro-ku, Tokyo 152-8551, Japan
* Correspondence: yudapn@itb.ac.id (Y.P.N.); uekusa@chem.titech.ac.jp (H.U.)

**Abstract:** Telmisartan is an anti-hypertensive drug that exhibits poor aqueous solubility. In this work, salt formation was utilized to address this issue. Three hydrochloride salts of telmisartan (TELHCl), a trihemihydrate hydrochloride salt (TELHCl-Hyd), and two anhydrate forms (TELHCl-A and TELHCl-B) were obtained. The crystal structures of TELHCl-Hyd and TELHCl-A were determined using single-crystal structure analysis. TELHCl-Hyd is a channel hydrate that has structural similarities with TELHCl-A. The structures of both crystals are mainly composed of chain structures formed by centrosymmetric dimers connected via carboxylic–benzimidazole hydrogen bonding. Despite their structural similarities, the dehydration of TELHCl-Hyd led to the formation of TELHCl-B. The solubility, intrinsic dissolution rate (IDR), powder flowability, and tabletability of TELHCl-Hyd and TELHCl-B were characterized and compared with those of the telmisartan free base form (TEL). The hydrochloride salts enhanced the solubility of telmisartan approximately 10 to 20 times and maintained the spring parachute effect up to 24 h. The IDR was also improved due to the existence of a hydrophilic channel that facilitates the dissolution of telmisartan cations. The resulting salts had a larger particle size and a more favorable crystal morphology that led to a better powder flowability. However, the tabletability was not improved by salt formation. The TEL exhibited a defined slip plane and a higher specific surface area that may assist the tableting process.

**Keywords:** telmisartan; crystal structure analysis; salt formation; hydrate; solubility; intrinsic dissolution; powder properties; flowability; tabletability; physicochemical properties



**Citation:** Nugraha, Y.P.; Unique, I.G.A.N.P.; Miyake, T.; Rahmah, R.; Indra, I.; Soewandhi, S.N.; Uekusa, H. Structural Characterization and Pharmaceutical Evaluation of Telmisartan Hydrochloride Salts. *Crystals* **2024**, *14*, 151. https://doi.org/10.3390/cryst14020151

Academic Editor: Tom Leyssens

Received: 27 December 2023
Revised: 24 January 2024
Accepted: 29 January 2024
Published: 31 January 2024



## 1. Introduction

Solubility is an important physicochemical factor that affects drug absorption and the effectiveness of drug therapy. Drugs that have a low solubility in water often exhibit low bioavailability and dissolution rates [1,2]. Telmisartan is an anti-hypertensive drug of the angiotensin receptor blocker (ARB) group categorized as BCS (biopharmaceutical classification system) class II, which means that this drug has a high permeability but low solubility [3]. One of the main problems of telmisartan is its very low solubility in biological solutions, causing slow dissolution and poor bioavailability [4].

Several studies have been conducted to improve the physicochemical properties of both the solubility and dissolution rate of the telmisartan free base form (TEL). Preparation of an amorphous solid dispersion (ASD) of telmisartan with various polymers using different techniques exhibited different structural and thermodynamic characteristics correlated with their physical stability and dissolution behavior. Dukeck et al. reported that telmisartan–eudragit ASD showed improved dissolution with a good physical stability due to its high interaction parameter [5]. Jamadar et al. used spray drying technology to produce telmisartan amorphous polymeric microparticles with PVP K30 with or without

the aid of an adsorbent [6]. The result showed that this technique significantly improved the solubility and dissolution rate of the drug due to amorphization and increased the specific surface area. A supercritical anti-solvent process was utilized by Park et al. to prepare a telmisartan solid dispersion with HPMC/PVP, resulting in amorphous solids with a reduced particle size. The solubility of the resulting ASD was increased with increasing amounts of polymers, while the dissolution decreased due to the formation of a gel layer in the polymer [7]. Isaac et al. improved the hydrophilicity and wettability of telmisartan by co-milling it with PVA, resulting a comparable dissolution profile with the reference product Micardis® [8]. In another report, amorphous telmisartan prepared through melt-quenching and cryogenic griding was formulated as tablet with a better flow and compression behavior during the tableting process compared to its crystalline counterpart [9].

Improvements in the physicochemical properties of telmisartan are also achieved by using a crystal engineering approach. Co-crystallization with oxalic acid increased the solubility of telmisartan 11.7-fold compared to the free base form [2]. Co-crystals with three different dissolution modes were obtained using various aromatic carboxylic acids in which using 2-hydroxybenzoic acid as a co-former showed a high dissolution performance trend in 0.1 M HCl due to a complexation with HCl solution [10]. Chadha et al. reported novel co-crystals of telmisartan with saccharin and glutaric acid [11]. Both cocrystals showed an improved solubility and bioavailability but underwent conversion into the free drug. In another study, the authors reported the formation of co-crystals between telmisartan and atenolol [12] with a two-fold increase in solubility in phosphate buffer pH 7.4, but it dissociated into its components. Another drug–drug co-crystal of telmisartan and febuxostat that has the potential to be utilized as a combination therapy has also been reported [13]. The cocrystal was found to be stable under an accelerated stability test, resulting in a decreased solubility and dissolution rate for each drug. Turek et al. recently published a review highlighting the role of co-crystallization in improving the physicochemical properties of ARBs including telmisartan [14].

In drug development, salt screening is considered to be a classical approach to improve the physicochemical properties of ionizable APIs [15]. Telmisartan has two benzimidazole groups and a carboxylic acid group, with pKa values of 4.57, 5.86 and 3.62, respectively [13]. Hence, salt formation with cationic or anionic counterions has the potential to be utilized on this compound. WO/2007/147889 and US 6737432 described the preparation of telmisartan salt with sodium [16] and organic acids [17]. Recently, Hatanaka et al. reported a co-amorphous drug–drug salt between telmisartan and amlodipine with an improved solubility and permeability for oral absorption [18]. Research has also been conducted to investigate the formation of telmisartan salt with the addition of hydrochloric acid (HCl), which shows an increase in solubility [19]. However, no further research has been conducted on the crystal structure of the salt formed, and no further characterization has been carried out.

In this study, salt formation of telmisartan with HCl was carried out to improve its physicochemical properties. A structural analysis of the resulting salt hydrochloride salt was conducted, followed by an investigation of its effect on the solubility, dissolution rate and powder properties.

## 2. Material and Methods

### *2.1. Materials*

TEL was from obtained as a gift from Dexa Medica (Palembang, Indonesia). Hydrochloric acid solution, potassium dihydrogen phosphate, sodium hydroxide and organic solvents were purchased from Merck Chemicals and Life Sciences (Jakarta, Indonesia) and Nacalai Tesque Inc. (Kyoto, Japan).

### 2.2. Preparation of Telmisartan Hydrochloride Salts (TELHCl)

The preparation method for telmisartan hydrochloride hydrate salt (TELHCl-Hyd) was adapted from a previous report [19]. A suspension of telmisartan free base (TEL) was prepared by adding 200 mg of TEL to 4 mL of ethanol. The suspension was mixed with 10 mL of 0.4 M HCl solution, stirred and heated at 40 °C for 1 h, resulting in a clear solution. The solution was filtered and left to evaporate at room temperature for two days, yielding TELHCl-Hyd salt crystals. A single crystal of TELHCl-Hyd (0.258 mm × 0.117 mm × 0.094 mm) was obtained using a similar method to prepare TELHCl-Hyd bulk crystals. However, instead of ethanol, water was used as the solvent. Plate-shaped crystals suitable for SCXRD were obtained in two weeks.

A plate-shaped single crystal (0.109 mm × 0.094 mm × 0.012 mm) of telmisartan hydrochloride anhydrate Form A (TELHCl-A) was obtained by recrystallizing TELHCl-Hyd in 1-propanol using the solvent evaporation method at room temperature. This anhydrous form will be discussed only in the crystal structure section. The synthesis of this form could not be repeated; hence, further characterization was not possible.

Telmisartan hydrochloride anhydrate Form B (TELHCl-B) was prepared by heating the powder of TELHCl-Hyd on a heating plate at 115 °C for 2 h. The resulting powders were kept in a desiccator until further characterization. We were not able to obtain a single crystal of TELHCl-B that was suitable for a single-crystal structure analysis.

### 2.3. Single-Crystal X-ray Diffraction (SCXRD)

XRD data for TELHCl-Hyd and TELHCl-A were collected at 93(2) K using a Rigaku R-AXIS RAPID II instrument (Rigaku, Tokyo, Japan) with rotating anode Cu-Kα radiation (λ = 1.541865 Å) in the ω-scan mode. An empirical absorption correction was performed using ABSCOR (Rigaku, Tokyo, Japan) [20] on the integrated and scaled diffraction data in RAPID-AUTO (Rigaku, Tokyo, Japan) [21]. The initial structure was solved using the dual space algorithm implemented in SHELXT (University of Göttingen, Göttingen, Germany) [22]. Structural refinement was completed in SHELXL (University of Göttingen, Göttingen, Germany) [23,24] using the full-matrix least square method. All non-hydrogen atoms were refined anisotropically. The hydrogen atoms of water molecules in TELHCl-Hyd were located in the difference Fourier maps. The other hydrogen atoms were treated in the riding model, and their displacement parameters were fixed to $1.2U_{eq}$ of the parent atoms. In TELHCl-A, the displacement parameters were fixed to $1.5U_{eq}$ of the parent oxygen atom or the parent carbon atoms in the methyl group. The diffraction intensity of TELHCl-A was weak due to the very small size of the single crystal. Therefore, we could not reduce the final *R* indices [$I > 2\sigma(I)$] $R_1 = 0.1629$.

Crystal structure visualization was conducted in Mercury 2023.3 [25] (CCDC, Cambridge, UK). The intermolecular interaction energy of TEL was calculated in CrystalExplorer v21.5 (University of Western Australia, Perth, Australia) [26] using CE-B3LYP model energy with B3LYP/6-31G(d,p) monomer electron densities to construct the energy framework. The scale factors for the electrostatic, polarization, dispersion and repulsion energies were 1.057, 0.740, 0.871 and 0.618, respectively.

### 2.4. Simultaneous Thermogravimetric and Differential Thermal Analysis (TG/DTA)

Simultaneous TG/DTA was performed using a STA7300 system (Hitachi, Tokyo, Japan) for TELHCl-Hyd. Approximately 3–5 mg of the sample was placed in an open aluminum pan and heated to 300 °C at 10 °C $min^{-1}$ under an $N_2$ purge of 60 mL $min^{-1}$. The empty pan was used as a reference. For the TEL samples, the measurement was conducted using a 9320 system (Rigaku, Tokyo, Japan) using identical measurement settings. Veusz 3.6.2 [27] was used to visualize the thermal analysis data.

### 2.5. Powder X-ray Diffraction

PXRD data were collected using a Bruker D8 Advance powder diffractometer (Bruker, Karlsruhe, Germany) equipped with a LYNXEYE XE detector using CuKα radiation

(λ = 1.54060 Å) generated at 40 kV and 20 mA. The sample was placed on a standard PMMA sample holder and scanned over 2θ = 2–50° at 5° $min^{-1}$ with a step size of 0.020°. The diffraction data were analyzed in Winplotr version March 2021 (University of Rennes, Rennes, France) [28].

### *2.6. Solubility and Intrinsic Dissolution Study*

A solubility study was employed using the shake flask method. Approximately 20 mg of each sample was added into a 50 mL pH 7.5 phosphate buffer medium. The flask was continuously shaken using an orbital shaker in a water bath, maintaining a constant temperature of 37 ± 0.5 °C. An aliquot of approximately 5 mL was taken at designated sampling times (3, 6, 9, 24 and 48 h).

Dissolution experiments were conducted using the rotating disk method employing a Hanson Research SR8-Plus dissolution tester. Approximately 200 mg of TEL and its salts was compressed into 8 mm discs. The dissolution experiments were conducted in 900 mL of pH 7.5 phosphate buffer medium at 37 ± 0.5 °C. The rotating disk apparatus was rotated at 75 rpm. At regular time intervals (15, 30, 45, 60, 75, 90, 115 and 120 min), a 10 mL aliquot was withdrawn from the vessel and filtered through a 0.45 µm cellulose acetate filter. Subsequently, 10 mL of pre-warmed medium was added to the vessel. For the dissolution and solubility study, each experiment was conducted in triplicate and the results were averaged.

The calibration curve using an external standard method was used to determine the concentration of telmisartan in the dissolution and solubility samples. The absorbance of each sample was measured at 297 nm using a UV–vis spectrophotometer (Beckman Coulter DU-720, Beckman Coulter, Inc, Brea, CA, USA).

### *2.7. Powder Characterization*

The flowability, particle size distribution and morphology of the TEL, TELHCl-Hyd and TELHCl-A crystals were characterized. The flowability was evaluated using the flow through an orifice method [29]. Approximately 25 g of powder was carefully placed into the disc cylinder. The diameter of the orifice was more than two times the diameter of the orifice opening. In addition, the diameter of the opening was more than six times the diameter of the particles. The powder flow rate was measured as the time it took for the powder to pass through the orifice.

The particle size distribution was measured using a laser diffraction method employing a Mastersizer 3000 (Malvern Panalytical, Malvern, UK). The wet dispersion method was employed. Before the measurement, pre-treatment was conducted to minimize the aggregation of the powder. Approximately 10 mg of sample and 0.05 µL of polysorbate 80 was added into 10 mL of water. The suspension was degassed and sonicated for 1 min. The sample suspension was placed into the Hydro MV wet disperser (Malvern Panalytical, Malvern, UK) unit and stirred at 1000 rpm. The measurement was conducted in six sequences with an obscuration limit of 2–8%. The volume diameter (Dv) for each sample was analyzed. All the measurement procedures were validated according to the USP 44 <429> light diffraction measurement of particle size [30].

The shape and morphology of the powder were studied using a scanning electron microscope (SEM) JSM-6510 LA (JEOL Ltd., Tokyo, Japan). Using a carbon double-sided adhesive tape, the powder samples were mounted onto an aluminum stub and sputter-coated with gold. The samples were scanned with an accelerating voltage of 15 kV.

### *2.8. Tabletability Study*

The tabletability was evaluated based on the samples' compaction behavior. Weighed powders (300 ± 10 mg) of the samples were compressed for a minute under a manual hydraulic press (Perkin Elmer, Waltham, MA, USA) into tablets with a diameter of 12 mm. The compression force ranged from 4.9 to 29.4 kN. After compaction, all the tablets were allowed to relax at room temperature for 24 h before subsequent experiments. The di-

mensions of the tablets were measured using calipers (Mitutoyo, Kawasaki, Japan). The breaking force of the tablets was measured using a tablet hardness tester (Biobase THT-3, Jinan, China). The tensile strength was calculated to eliminate the effects of the variable thickness and diameter on the measured breaking force using the following equation [31]:

$$\sigma_t = \frac{2F}{\pi D t}$$

where $\sigma_t$ is the tensile strength (MPa), $F$ is the breaking force (N), $D$ is the diameter of the tablet (mm) and $t$ is the thickness of the tablet (mm).

## 3. Results and Discussion

### *3.1. Crystal Structure of Telmisartan HCl Salts*

We obtained a crystalline powder after the solvents evaporated and crystallized. The resulting powder showed a different PXRD pattern compared to the TEL diffractogram (Figure 1).

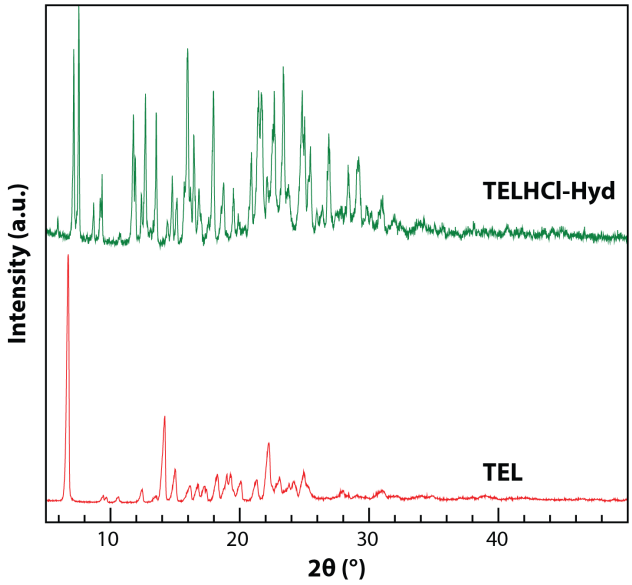


**Figure 1.** PXRD pattern of TEL and TELHCl-Hyd.

In addition, as shown in Figure 2, the resulting powder had a distinct particle shape compared to the rod-shaped TEL raw material. Further characterization revealed that the resulting powder was a hydrochloride salt hydrate of telmisartan (TELHCl-Hyd).

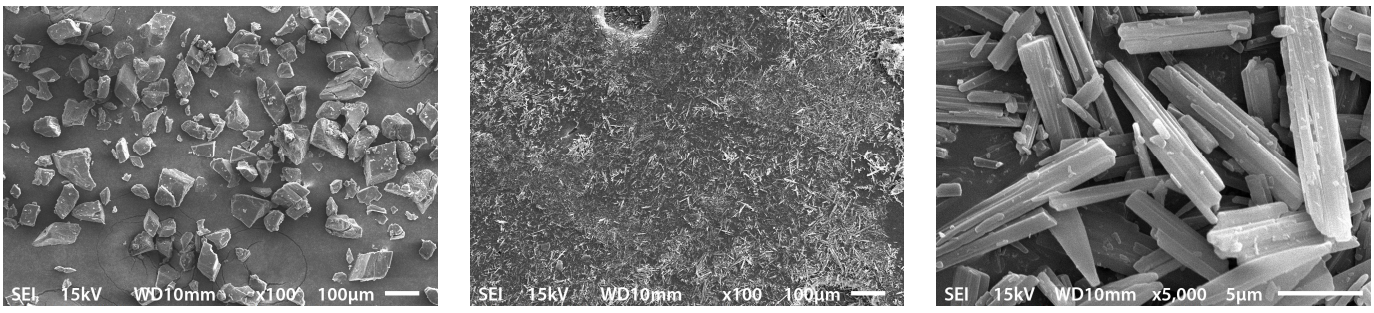


(**a**) (**b**) (**c**)

**Figure 2.** SEM photograph of (**a**) TELHCl-Hyd and (**b**) TEL crystals at 100× magnification. (**c**) SEM photograph of TEL crystals at 5000× magnification.

We successfully analyzed the crystal structure of TELHCl-Hyd. For a comparison of the crystal structure, we refer to the published structure of TEL Form A [32]. The crystal data and refinement details are summarized in Table 1.

**Table 1.** Crystallographic data and refinement details of TEL Form A, TELHCl-Hyd and TELHCl-A.

| Parameter | TEL Form A † | TELHCl-Hyd | TELHCl-A |
|---|---|---|---|
| Moiety formula | $C_{33}H_{30}N_4O_2$ | $C_{33}H_{31}ClN_4O_2{\cdot}3.5(H_2O)$ | $C_{33}H_{31}ClN_4O_2$ |
| Formula weight | 514.63 | 614.2 | 551.07 |
| Calc. density (g cm$^{-3}$) | 1.24 | 1.319 | 1.317 |
| Crystal system | Monoclinic | Triclinic | Monoclinic |
| Space group | $P2_1/c$ | $P$-1 | $P2_1/c$ |
| $a$ (Å) | 18.7798(3) | 12.7169(3) | 13.2201(3) |
| $b$ (Å) | 18.1043(2) | 16.1019(3) | 16.2647(3) |
| $c$ (Å) | 8.00578(7) | 16.1871(3) | 25.8530(6) |
| $\alpha$ (°) | 90 | 95.0040(10) | 90 |
| $\beta$ (°) | 97.066(1) | 110.1320(10) | 91.4510(10) |
| $\gamma$ (°) | 90 | 91.7840(10) | 90 |
| Volume (Å$^3$) | 2701.31 | 3093.56(11) | 5557.2(2) |
| $Z$, $Z'$ | 4, 1 | 4, 2 | 8, 2 |
| $T$ (K) | 295 | 93(2) | 93(2) |
| Measured ref. | - | 35,576 | 64,180 |
| Independent ref. | - | 11,114 [$R_{(int)}$ = 0.0779] | 10,171 [$R_{(int)}$ = 0.2060] |
| Refined parameter | - | 874 | 731 |
| Goodness-of-fit on $F^2$ | - | 1.048 | 0.989 |
| Final $R$ indices [$I > 2\sigma(I)$] | - | $R_1$ = 0.0805 | $R_1$ = 0.1629 |
| CCDC deposit number | 209,544 | 2,320,400 | 2,320,398 |

† Data originated from structure determination based on powder X-ray diffraction (SDPD) by Dinnebier et al. [32].

TELHCl-Hyd crystallizes in the triclinic $P$-1 space group comprising two telmisartan cations, two chloride anions, and seven water molecules (Figure 3a). Both telmisartan molecules are protonated on the N2 and N6 positions of the benzimidazole, respectively. Hence, TELHCl-Hyd is a trihemihydrate ($3.5H_2O$) hydrochloride salt of telmisartan. Meanwhile, both symmetry-independent telmisartan cations share similar conformations despite their conformational flexibility, as shown in Figure 3b. The cations exist with a disorder in the propyl group of the benzimidazole ring. The occupancy factors of the major disordered parts of both independent telmisartan cations are refined as 0.66 and 0.57, respectively.

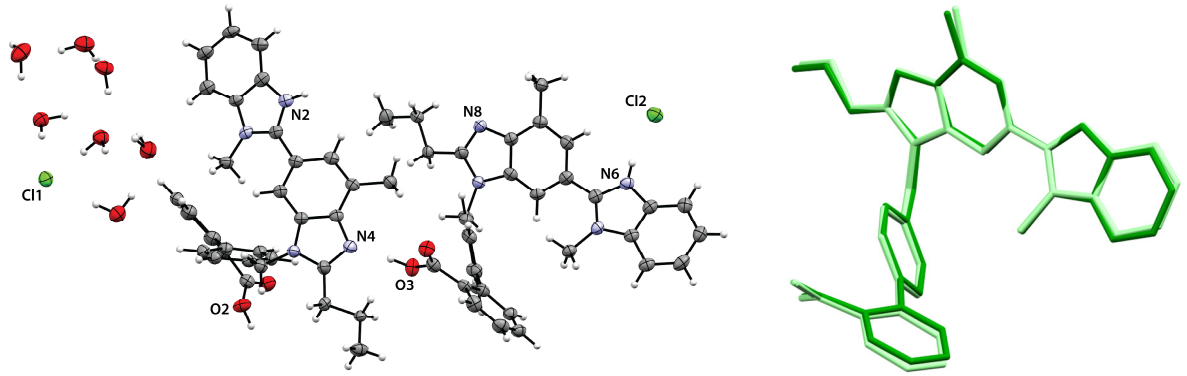


(**a**) (**b**)

**Figure 3.** (**a**) Thermal ellipsoid drawing of TELHCl-Hyd at a 50% probability level. Only the atoms involved in the hydrogen bonding described are labeled for clarity. (**b**) Overlay of the two asymmetric cations of TELHCl-Hyd. Hydrogen atoms and minor disordered parts are omitted for clarity.

In this crystal, only one chloride ion is involved in direct charge-assisted N6–H6···Cl2 hydrogen bonding with the telmisartan cation. Furthermore, each asymmetric telmisartan

cation forms a centrosymmetric dimer-like structure connected by T-shaped π···π interaction, with distances between the ring centroid of 5.087 and 5.185 Å, respectively (Figure S1). These dimers are connected through carboxylic–benzimidazole hydrogen bonding interactions O3–H3B···N4 and O2–H2A···N8, forming a one-dimensional chain along the *a*-axis, as depicted in Figure 4a.

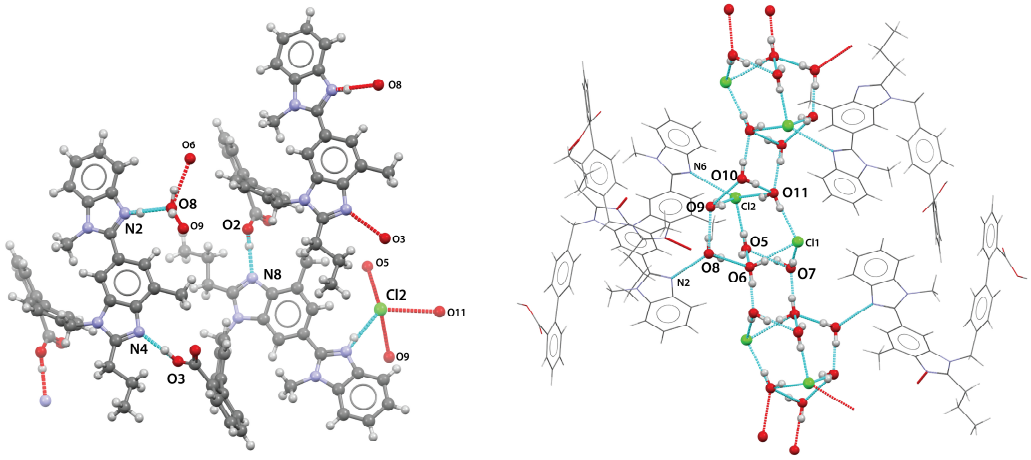


**Figure 4.** (**a**) Hydrogen bonding motif in TELHCl-Hyd highlighting the interaction between each molecule in the asymmetric unit. Only the atoms involved in the hydrogen bonding described are labeled for clarity. (**b**) Extensive hydrogen bonding between water molecules along the *b*-axis in TELHCl-Hyd.

Interestingly, all seven water molecules were located close to each other, forming a cluster of hydrates with extensive intermolecular hydrogen bonding (Figure 4b). Five water molecules, i.e., O5, O7, O8, O9 and O10, were involved as donors in two hydrogen bonds and as an acceptor in one hydrogen bond. On the other hand, O6 and O11 took part in four hydrogen bond interactions. Only one water molecule (O8) was involved in hydrogen bonding with the telmisartan molecule. The hydrogen bond details are summarized in Table 2.

**Table 2.** Hydrogen bond parameters in TELHCl-Hyd.

| D–H···A | D–H (Å) | H···A (Å) | D···A (Å) | D–H···A (°) |
|---|---|---|---|---|
| N2–H2B···O8 | 0.88 | 1.85 | 2.728(5) | 172.4 |
| N6–H6···Cl2 | 0.88 | 2.22 | 3.087(3) | 169.0 |
| O2–H2A···N8 [a] | 0.95 | 1.71 | 2.646(4) | 169.2 |
| O3–H3B···N4 | 0.96 | 1.68 | 2.6318(14) | 170.5 |
| O5–H5A···Cl2 [b] | 0.9570(11) | 2.265(7) | 3.218(3) | 174(5) |
| O5–H5B···O6 | 1.017(7) | 1.8435(10) | 2.785(4) | 152.4(13) |
| O6–H6A···Cl1 | 0.9571(10) | 2.292(7) | 3.238(3) | 170(3) |
| O6–H6B···O7 | 0.973(6) | 1.7682(10) | 2.738(4) | 174(4) |
| O7–H7E···O5 [c] | 0.972(9) | 1.958(8) | 2.868(4) | 155(2) |
| O7–H7D···Cl1 [c] | 0.953(10) | 2.241(15) | 3.177(3) | 167(4) |
| O8–H8A···O6 | 0.955(10) | 1.88(2) | 2.796(4) | 161(5) |
| O8–H8B···O9 | 0.957(10) | 1.855(19) | 2.782(5) | 162(5) |
| O9–H9A···Cl2 [b] | 0.968(10) | 2.247(15) | 3.203(3) | 169(5) |
| O9–H9B···O10 | 0.955(10) | 2.11(4) | 2.827(5) | 131(4) |
| O10–H10A···O11 | 0.960(10) | 1.93(3) | 2.831(4) | 156(5) |
| O10–H10B···O11 [d] | 0.967(9) | 1.955(9) | 2.911(5) | 169(4) |
| O11–H11A···Cl2 [b] | 0.954(10) | 2.226(16) | 3.159(3) | 166(4) |
| O11–H11B···Cl1 | 0.954(10) | 2.247(13) | 3.192(3) | 171(4) |

Symmetry transformations: [a] x + 1, y, z; [b] x, y, z − 1; [c] −x, −y + 2, −z; [d] −x, −y + 1, −z.

Consequently, hydrophilic channels consisting of water molecules and chloride ions along the *b*-axis were formed (Figure 5). Using Hydrate Analyzer in Mercury, we found that these channels occupied 15.5% of the unit cell volume.

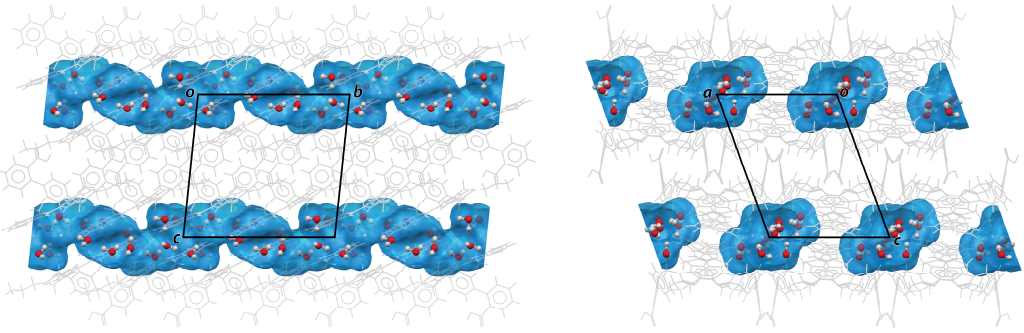


(**a**) (**b**)

**Figure 5.** Water molecule channels on TELHCl-Hyd viewed along (**a**) the *a*-axis and (**b**) the *b*-axis.

TELHCl-A exists in the monoclinic space group $P2_1/c$. The asymmetric unit of this crystal consists of two telmisartan cations and two chloride anions (Figure 6a). In general, both cations have a similar conformation with those of TELHCl-Hyd. Only the propyl group of the benzimidazole of one cation has a different conformation due to its dihedral angle, as shown in Figure 6b. TELHCl-A also has identical intermolecular interactions between each telmisartan cation, comprising a one-dimensional chain along the *a*-axis that is formed by carboxylic–benzimidazole interactions (O2···N8 and O3···N4), as depicted in Figure 6c. However, in this crystal, both chloride anions formed a charge-assisted hydrogen bond with the protonated telmisartan via N6–H6···Cl1 and N2–H2B···Cl2 interactions. The hydrogen bond parameters of TELHCl-A are summarized in Table 3.

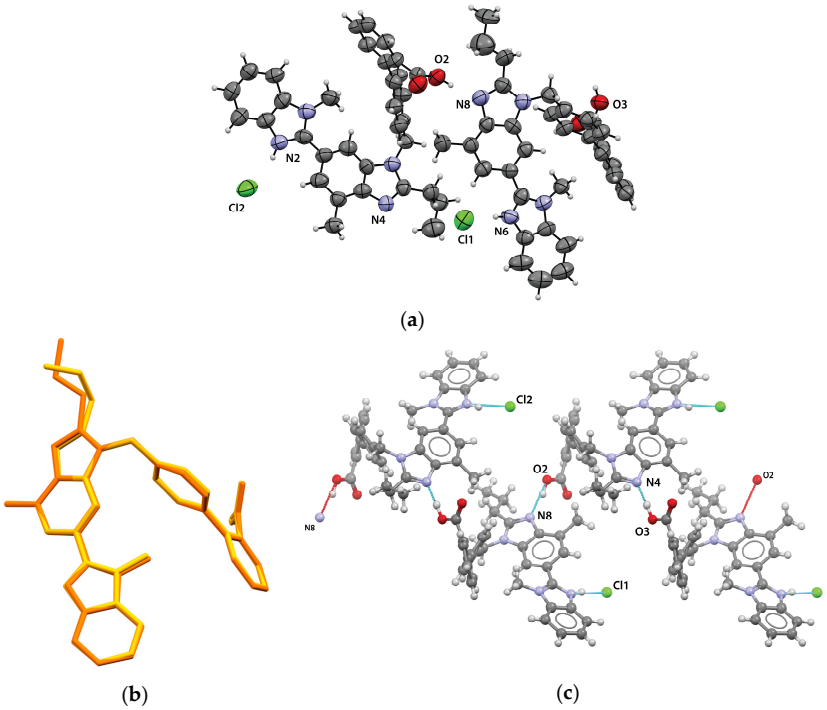


(**a**)

(**b**) (**c**)

**Figure 6.** (**a**) Thermal ellipsoid drawing of TELHCl-A at a 50% probability level. Only the atoms involved in the hydrogen bonding described are labeled for clarity. (**b**) Overlay structure of telmisartan cations in TELHCl-A. Hydrogen atoms are omitted for clarity. (**c**) Hydrogen bonding motif in TELHCl-A highlighting the interactions between each molecule in the asymmetric unit forming a 1-D chain structure. Only the atoms involved in the hydrogen bonding described are labeled.

**Table 3.** Hydrogen bond parameters in TELHCl-A.

| D–H···A | D–H (Å) | H···A (Å) | D···A (Å) | D–H···A (°) |
|---|---|---|---|---|
| O2-H2A···N8 [a] | 0.96 | 1.76 | 2.6912(17) | 164.4 |
| O3-H3B···N4 [c] | 0.96 | 1.67 | 2.614(8) | 167.8 |
| N2-H2B···Cl2 [b] | 0.88 | 2.14 | 2.998(8) | 163.5 |
| N6-H6···Cl1 | 0.88 | 2.12 | 2.995(7) | 170.7 |

Symmetry transformations: [a] x, −y + 1/2, z + 1/2; [b] −x, y − 1/2, −z + 1/2; [c] x + 1, −y + 1/2, z − 1/2.

### *3.2. Thermal Analysis and Dehydration Behavior of Telmisartan HCl Salts*

Subsequently, a thermal analysis of TEL and TELHCl-Hyd was carried out. The TG–DTA curve of TEL is shown in Figure 7a. A sharp endothermic peak at 268.7 °C corresponds to the melting of the higher melting point polymorph of TEL Form A. The stable TEL Form A was reported to undergo melting at 263–272 °C [5,8,9,33–35].

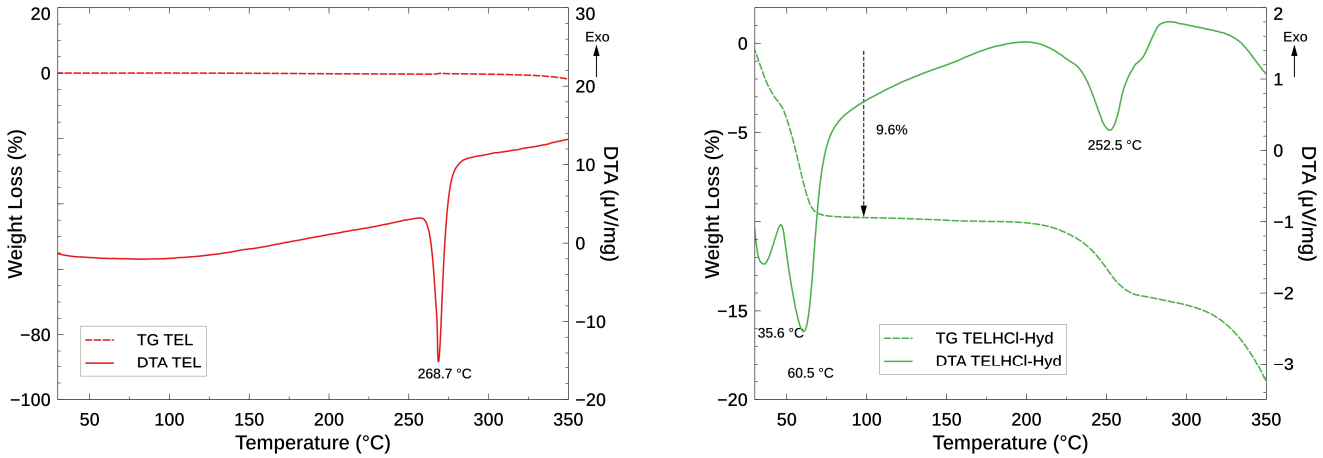


**Figure 7.** Thermal behavior of TEL (**a**) and TELHCl-Hyd (**b**). Solid line indicates the differential thermal analysis (DTA) curve. Dashed line corresponds to the thermogravimetric (TG) curve. The temperature label in both figures is the temperature of the peak maximum.

We also confirmed via PXRD that the crystal form of the TEL raw material used in this study was TEL Form A (Figure 8a). The TG–DTA data for the hydrate hydrochloride salt of telmisartan are shown in Figure 7b. Upon heating, this phase showed an immediate weight loss of ca. 9.6%, associated with two overlapping endothermic peaks at 35.6 and 60.5 °C. This thermal event corresponds to the loss of 3.5 moles of water molecules (10.3%) per mole of TELHCl, in agreement with the TELHCl:$H_2O$ ratio in the crystal structure, i.e., 2:7. Another broad endothermic peak at 252.6 °C with two steps of significant weight loss was observed after further heating. This event represents melting followed by a decomposition process [34,35].

The transformation or dehydration of TELHCl-Hyd occurred within a relatively low temperature range. In other words, water molecules were easily removed from the crystal. Dehydration at a low temperature is a typical behavior of channel hydrates [36,37]. As described in the previous section, TELHCl-Hyd is a channel hydrate. In addition, only one of the seven water molecules in the asymmetric unit was directly connected with the telmisartan cation. Hence, these two structural features are responsible for the facile dehydration of TELHCl-Hyd.

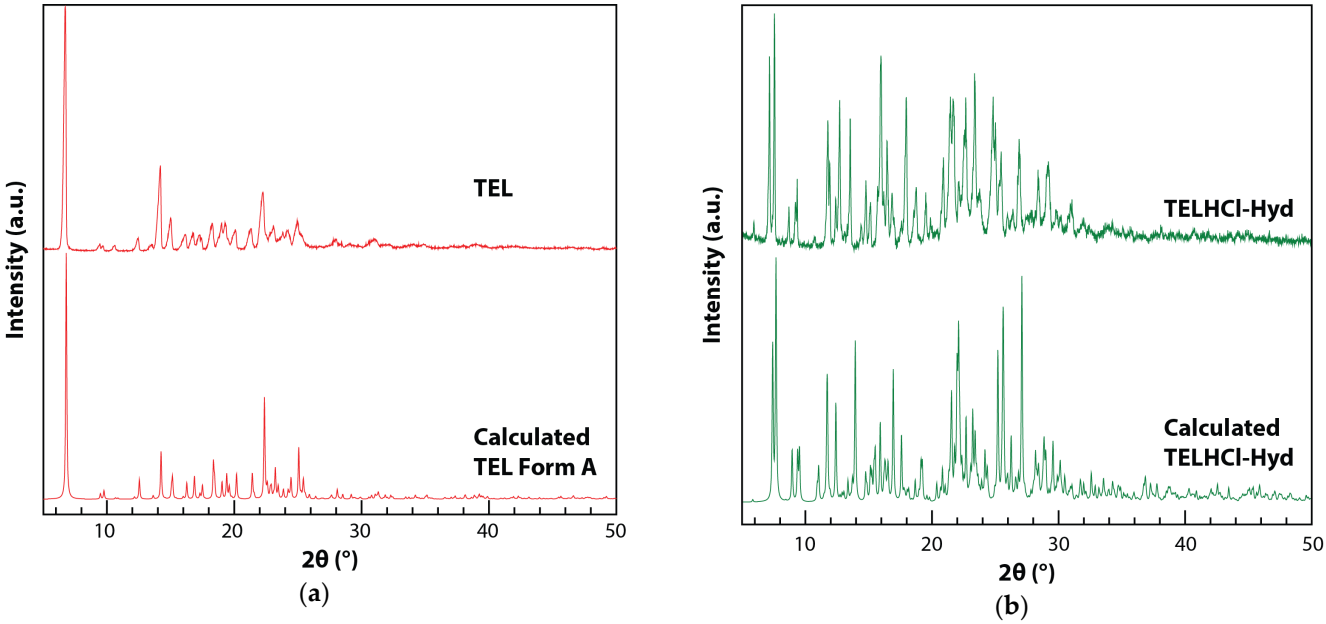


**Figure 8.** Comparison between experimental and simulated powder pattern of (**a**) TEL and (**b**) TELHCl-Hyd.

Following that, we analyzed the dehydration product of TELHCl-Hyd using PXRD. After heating TELHCl-Hyd at 115 °C for 2 h, a crystalline phase was obtained. Interestingly, this product has a different PXRD pattern compared to the calculated pattern of TELHCl-A (Figure 9). We concluded that upon heating, the removal of water molecules from TELHCl-Hyd led to the formation of a new anhydrous polymorph B or TELHCl-B. This behavior is counterintuitive. As shown in Figure 10, the crystal packing of TELHCl-Hyd and TELHCl-A is very similar. The packing index [38] of TELHCl-Hyd and TELHCl-Anh is not significantly different, at 69.5 and 68.9%, respectively. In addition, the telmisartan conformation is nearly identical in both crystals. However, despite their structural similarities, upon removal of water through heating, TELHCl-Hyd did not transform into TELHCl-A.

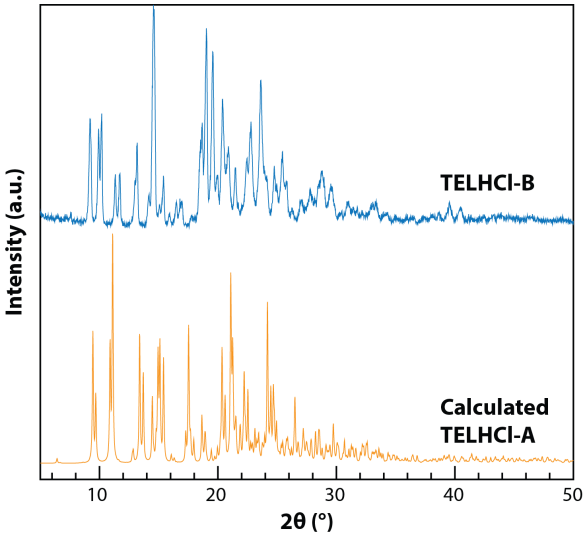


**Figure 9.** PXRD pattern of the TELHCl-B sample obtained by heating TELHCl-Hyd at 115 °C for 2 h (**top**) and simulated PXRD pattern of TELHCl-A from single-crystal data (**bottom**).

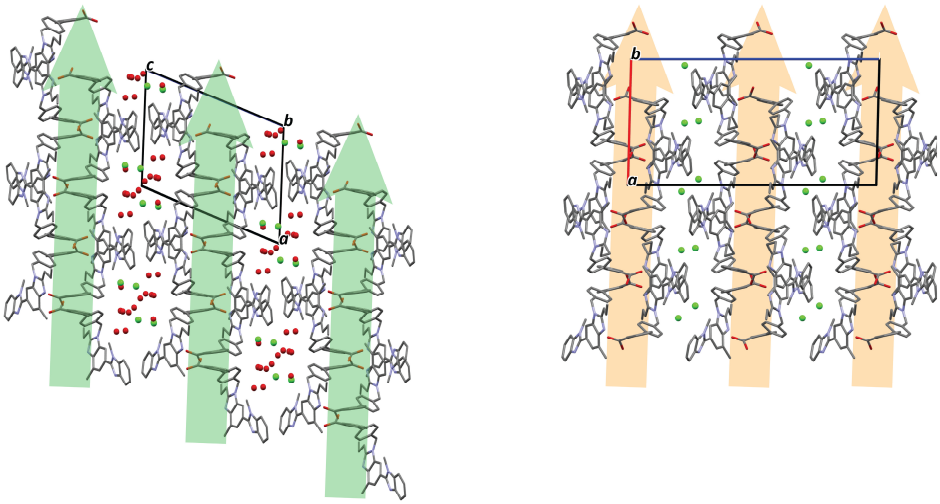


(**a**) (**b**)

**Figure 10.** Comparison between crystal packing of (**a**) TELHCl-Hyd and (**b**) TELHCl-A viewed along the *b*-axis. Hydrogen atoms are omitted for clarity.

In our previous report on the dehydration of metoclopramide HCl monohydrate [39], a major structural rearrangement occurred because the water molecules were critical in stabilizing the crystal structure. Thus, dehydration followed by melting and recrystallization processes was necessary to transform the monohydrate into the anhydrous form. As described above, the dehydration process of TELHCl-Hyd did not include a melting or recrystallization process, as no sharp endothermic or exothermic peak was observed. Therefore, in contrast with the isolated-site hydrate of metoclopramide HCl, the dehydration process of TELHCl-Hyd to TELHCl-B allows for only a minor structural rearrangement. We were not able to obtain a single crystal of TELHCl-B, but we hypothesize that the crystal structure of TELHCl-B would be similar to TELHCl-A. In addition, there was no visible difference between the shape and morphology of TELHCl-Hyd and TELHCl-B using SEM (Figure 11).

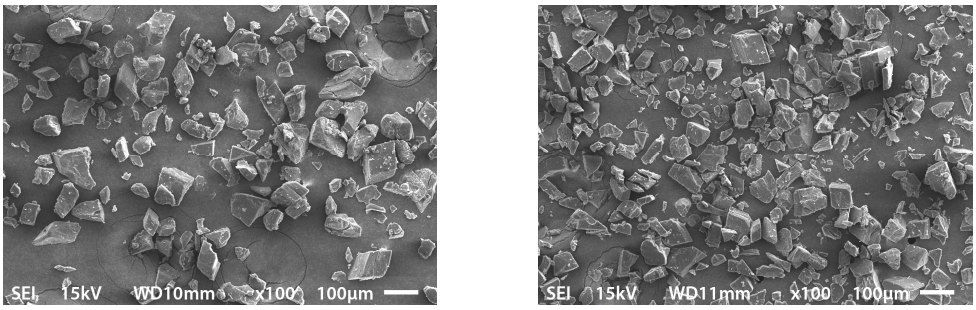


(**a**) (**b**)

**Figure 11.** SEM photograph of **(a)** TELHCl-Hyd and **(b)** TELHCl-B at 100× magnification.

It should be noted that no additional peak or thermal event was observed after the dehydration process except for the final melting/decomposition. We hypothesize that TELHCl-A could be obtained only through recrystallization of TELHCl-Hyd from the solvent. A more detailed study is planned to investigate the relationship between TELHCl-A, TELHCl-B, and TELHCl-Hyd.

### *3.3. Solubility and Intrinsic Dissolution Study*

Salt formation was aimed to improve the solubility of telmisartan. Thus, we evaluated the solubility and intrinsic dissolution of the resulting salts. Each study was conducted in pH 7.5 phosphate buffer in accordance with the dissolution of telmisartan tablets in

USP 44 [40]. Before we started the evaluation, we confirmed that the bulk powder for the characterization of TELHCl-Hyd was in the same phase as the single crystal (Figure 8b) using PXRD. The solubility and intrinsic dissolution curves of TEL and its salts are presented in Figure 12.

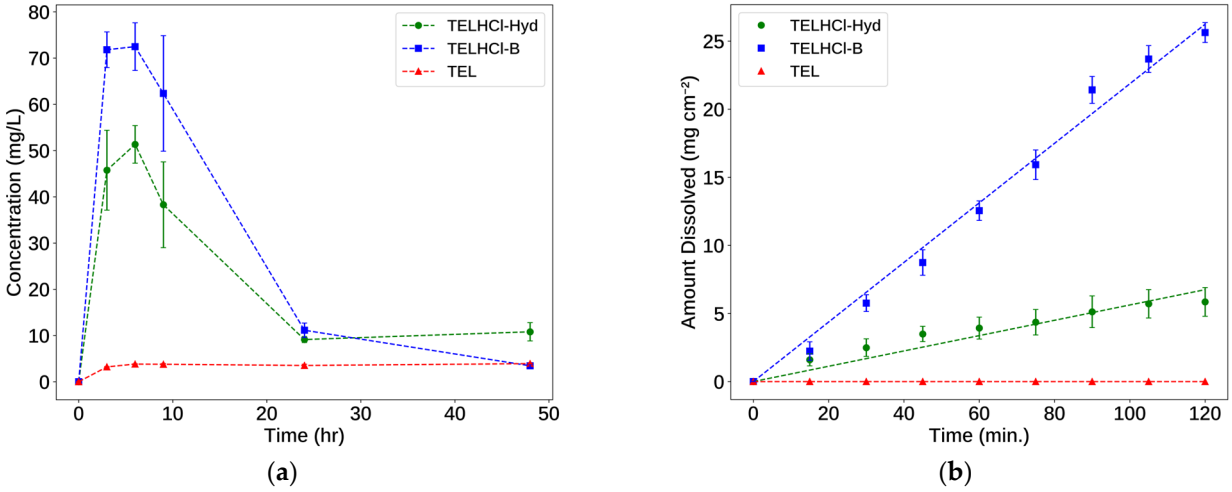


**Figure 12.** Solubility (**a**) and intrinsic dissolution (**b**) curves of TEL and TELHCl salts. Phosphate buffer pH 7.5 was used as the medium.

During the solubility study, the TEL sample reached its equilibrium concentration after 6 h. The equilibrium solubility of TEL was 3.83 ± 0.05 mg/L. The "spring and parachute" effect was observed in both salts. The concentration of TELHCl-Hyd and TELHCl-B increased up to 6 h and then continued to decrease slowly to the equilibrium concentration of TEL. The concentration or solubility of TELHCl-Hyd and TELHCl-B at 6 h was 51.33 ± 4.07 and 72.48 ± 5.14 mg/L, respectively. The spring and parachute effect is typically exhibited by the metastable form [41,42]. During the solubility study, conversion to the more stable form occurred. To analyze this occurrence, the residual powders after the solubility test were characterized using PXRD. The PXRD diffractogram is shown in Figure 13. The characteristic peaks of TEL were observed in both the hydrate and anhydrate salt samples. Furthermore, the TELHCl-B residual sample also showed TELHCl-Hyd-characteristic peaks. While TELHCl-B underwent a complete transformation, forming a TELHCl-Hyd and TEL mixture, the TELHCl-Hyd partially transformed into the free base form. This result suggested that transformation from TELHCl-B to TELHCl-Hyd occurred before the recrystallization of TEL. In this study, the bulk precipitation mechanism of the free base occurred because the precipitation or recrystallization of TEL took place above the critical concentration [43]. Similar behavior during the solubility test was observed in telmisartan–phthalic acid co-crystals [4]. At a pH > 6, a cocrystal and telmisartan mixture was obtained after the solubility test.

The intrinsic dissolution rates (IDRs) of TELHCl-Hyd and TELHCl-B are 0.056 and 0.219 mg $min^{-1}$ $cm^{-2}$, respectively. Over the course of the IDR study, TEL was practically insoluble. The IDR results show a good correlation with the solubility study. According to the classification by Yu et al. (2004) [44], TELHCl-B can be considered as a highly soluble compound (IDR > 0.1 mg $min^{-1}$ $cm^{-2}$). This anhydrous form dissolves four times faster compared to TELHCl-Hyd. Hydrate forms are generally known to have lower solubilities compared to their anhydrous counterparts due to their higher stability [45]. The higher stability of TELHCl-Hyd was demonstrated during the solubility test. Compared to TEL, TELHCl-Hyd shows a significant improvement in its IDR. It is expected that due to the channel structure of TELHCl-Hyd, the water molecules readily escaped from the crystal. Hence, this hydrophilic channel may facilitate the inclusion of the dissolution medium into the crystal and dissolve the telmisartan cations.

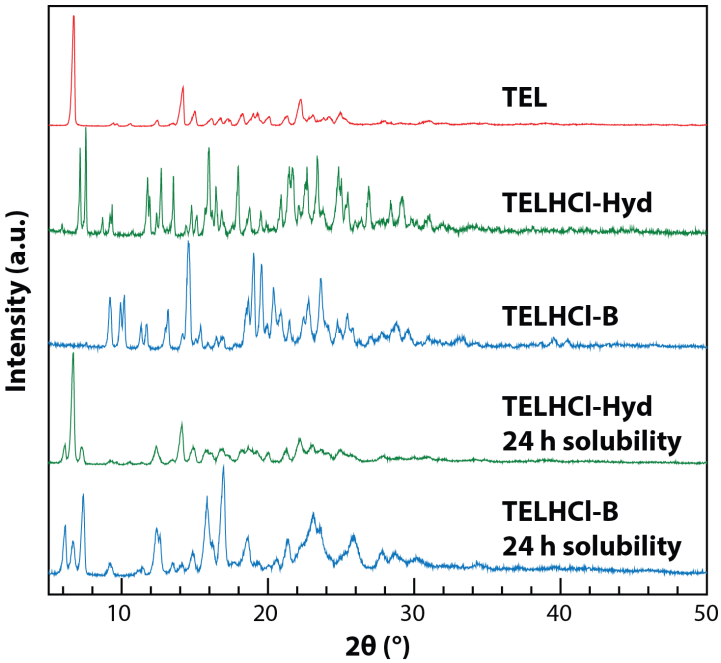


**Figure 13.** PXRD pattern of the residual samples after the solubility experiment.

### *3.4. Powder Characterization and Tabletability*

Lepek et al. reported that tablet blends containing crystalline TEL and excipients had a very poor flowability during a tableting process. Similarly, Ratih et al. also reported on the poor flow characteristics of TEL [3]. We experienced a similar problem in this study and in our previous work with TEL [46]. TEL exists as a very fine rod-like particle ($Dv_{50}$ = 3.9 µm), which leads to its poor flowability. Hence, in this research, we characterized the powder properties of TEL and its salts. The results of the powder characterization are presented in Table 4.

**Table 4.** Particle size and powder flowability of TEL, TELHCl-Hyd and TELHCl-B powders.

| Sample | Average Particle Size [a] ($Dv_{50}$, µm) | Powder Flow [b] (g $s^{-1}$) |
|---|---|---|
| TEL | 3.90 ± 0.48% | 1.13 ± 0.01 |
| TELHCl-Hyd | 31.97 ± 2.79% | 11.40 ± 0.15 |
| TELHCl-B | 32.42 ± 0.43% | 8.38 ± 0.22 |

[a] Value is expressed as mean ± RSD; [b] value is expressed as mean ± SD.

Compared to the free base, the hydrochloride salts of telmisartan exhibited a significantly better flowability. Apart from the larger particle size, salt formation also altered the shape of the particles. The flowability is influenced by the shape of the particles. Particles with a similar spherical size tend to have a better flowability [47,48]. Observed using SEM, the TEL powders were found to be an agglomerate of fine rod-like particles, while both salts were relatively more cuboid. We concluded that the changes in the size and shape of the particles were responsible for the better flowability of TELHCl-Hyd and TELHCl-B.

Finally, we evaluated the powder compaction behavior of TEL and its salts. The relationship between the compaction force and tensile strength is presented in Figure 14.

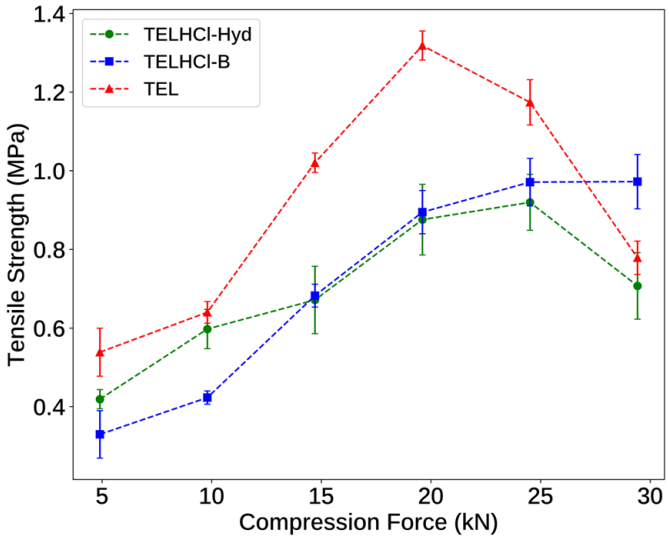


**Figure 14.** Tabletability of TEL and TELHCl salts.

Tabletability is an important property related to the processability of API in solid dosage form development. This characteristic represents the capacity of a material to be transformed into a tablet of a specific strength under compaction pressure [49]. The tensile strength of TEL remained higher than TELHCl-Hyd and TELHCl-B at all the applied compression forces. This result indicates the better tabletability of TEL over its salts. At compression forces higher than 20 kN, overcompression occurred. The observed decrease in the tensile strength was attributed to an excessive elastic recovery [50].

The superior tabletability of TEL can be rationalized from its crystal structure. The existence of slip planes is reported to enhance the tabletability of APIs [51–57]. Slip planes correspond to the crystallographically rigid planes exhibiting the weakest interactions between planes [58]. We identified the possible slip plane by constructing the energy framework [26] and visualizing the crystal structure using the CSD Particle module in Mercury [25]. TEL exists as a layered structure connected by head-to-tail carboxylic–benzimidazole hydrogen bonding along the *c*-axis. This structure has a defined slip plane parallel to the (1 0 0) plane, as shown in Figure 15a. The slip planes are separated by relatively weaker hydrophobic interactions. The existence of these defined planes facilitated shearing and allowed the structure to easily slide, thereby promoting plastic deformation. On the other hand, despite the existence of a layered structure in TELHCl-Hyd, this structure lacks a slip plane due to the water channel separating the stacked layers. This water channel bridges the adjacent layers through telmisartan–water hydrogen bonding (Figure 15b). This creates an interlocking structure that hinders plastic deformation during the compression process. In addition to the crystal packing, the larger particle size of the corresponding salts also influenced their tabletability. Several studies have reported that smaller particles tend to have better tabletability due to their larger specific surface area, facilitating bonding between particles [59–61]. Compared to a previous study on the tabletability of TEL using a similar method [3], in this work, TEL showed a marginally better tabletability. This may be attributed to the slightly lower particle size distribution of the TEL used in this research compared to the previous report ($Dv_{50}$ = 4.2 µm).

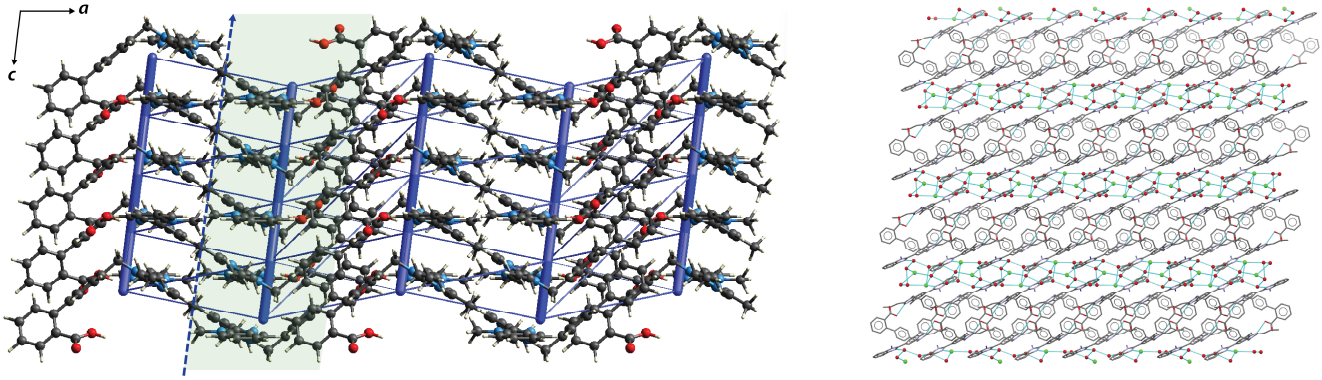


(**a**) (**b**)

**Figure 15.** (**a**) Energy framework of the TEL crystal structure viewed along the *b*-axis. The intermolecular energy cut-off was set to 5 kJ/mol. The layer comprised of hydrogen bonding along the *c*-axis is highlighted in green. The possible slip plane (1 0 0) is shown as a dashed blue line. (**b**) Crystal packing of TELHCl-Hyd viewed along the *a*-axis.

## 4. Conclusions

Hydrochloride salts of telmisartan were successfully synthesized and characterized. The resulting salts were a trihemihydrate (TELHCl-Hyd) and two anhydrate forms (TELHCl-A and TELHCl-B). Despite its structural similarities, the channel hydrate TELHCl-Hyd did not transform into TELHCl-A upon dehydration. In contrast, TELHCl-B was obtained as the dehydration product of TELHCl-Hyd. Further investigation is necessary to understand the thermodynamic relationship between the anhydrate forms. Salt formation was able to increase the solubility of telmisartan by 10–20-fold and maintained the spring and parachute effect up to 24 h. Recrystallization to the free base form occurred during the solubility test due to the stability of TEL. The intrinsic dissolution rate of telmisartan is improved by salt formation due to the existence of a hydrophilic channel, facilitating the dissolution of telmisartan cations in TELHCl-Hyd. The hydrochloride salts exhibited a better powder flowability due to the larger particle size distribution and the change in its crystal shape, which were more favorable than the rod-like crystal of TEL. However, TEL showed a better tabletability compared to its corresponding salts due to the existence of a defined slip plane. A higher surface area that facilitated interparticulate bonding also contributed to TEL's tabletability. This work emphasizes the role of salt formation in improving the solubility, dissolution rate and powder properties of poorly soluble APIs.

**Supplementary Materials:** The following supporting information can be downloaded at: https://www.mdpi.com/article/10.3390/cryst14020151/s1, Figure S1: Centrosymmetric dimer structure in TELHCl-Hyd.

**Author Contributions:** Conceptualization, Y.P.N. and H.U.; methodology, Y.P.N., S.N.S. and H.U.; validation, Y.P.N. and S.N.S.; formal analysis, Y.P.N.; investigation, I.G.A.N.P.U., T.M., R.R. and I.I.; writing—original draft preparation, Y.P.N. and I.G.A.N.P.U.; writing—review and editing, Y.P.N. and H.U.; visualization, Y.P.N., I.G.A.N.P.U. and R.R.; supervision, project administration and funding acquisition, Y.P.N., S.N.S. and H.U. All authors have read and agreed to the published version of the manuscript.

**Funding:** Part of this work was funded by the Institute for Research and Community Services (LPPM) Bandung Institute of Technology through Riset Peningkatan Kapasitas Dosen Muda ITB Program 2023, grant number 308/IT1.B07.1/TA.00/2023. Part of this work was supported by JSPS KAKENHI Grant Number JP20H04661 and JP22K05032 (H.U.).

**Data Availability Statement:** The data presented in this study are available in this paper and its supplementary information. The crystal structures (crystallographic information file, .cif) of TELHCl-Hyd and TELHCl-A can be publicly accessed through the Cambridge Structural Database

(https://www.ccdc.cam.ac.uk/structures) with the deposition numbers 2,320,400 and 2,320,398, respectively.

**Acknowledgments:** The authors are grateful to Dexa Medica Indonesia for the telmisartan donation. Y.P.N. sincerely appreciates JASSO for the Follow-Up Research Fellowship. Assistance from the Kimia Farma Research Centre with the particle size measurements is also acknowledged.

**Conflicts of Interest:** The authors declare no conflicts of interest.

## References

1. Bhalani, D.V.; Nutan, B.; Kumar, A.; Singh Chandel, A.K. Bioavailability Enhancement Techniques for Poorly Aqueous Soluble Drugs and Therapeutics. *Biomedicines* **2022**, *10*, 2055. [CrossRef] [PubMed]
2. Alatas, F.; Ratih, H.; Soewandhi, S.N. Enhancement of Solubility and Dissolution Rate of Telmisartan by Telmisartan-Oxalic Acid Co-Crystal Formation. *Int. J. Pharm. Pharm. Sci.* **2015**, *7*, 423–426.
3. Ratih, H.; Pamudji, J.S.; Alatas, F.; Soewandhi, S.N. Improving Telmisartan Mechanical Properties through the Formation of Telmisartan and Oxalic Acid Co-Crystal by Slow Evaporation and Ultrasound Assisted Co-Crystallization from Solution Methods. *Songklanakarin J. Sci. Technol.* **2020**, *42*, 188–195. [CrossRef]
4. Kundu, S.; Kumari, N.; Soni, S.R.; Ranjan, S.; Kumar, R.; Sharon, A.; Ghosh, A. Enhanced Solubility of Telmisartan Phthalic Acid Cocrystals within the pH Range of a Systemic Absorption Site. *ACS Omega* **2018**, *3*, 15380–15388. [CrossRef] [PubMed]
5. Dukeck, R.; Sieger, P.; Karmwar, P. Investigation and Correlation of Physical Stability, Dissolution Behaviour and Interaction Parameter of Amorphous Solid Dispersions of Telmisartan: A Drug Development Perspective. *Eur. J. Pharm. Sci.* **2013**, *49*, 723–731. [CrossRef] [PubMed]
6. Jamadar, S.; Pore, Y.; Sayyad, F. Formation of Amorphous Telmisartan Polymeric Microparticles for Improvement of Physico-chemical Characteristics. *Part. Sci. Technol.* **2014**, *32*, 512–519. [CrossRef]
7. Park, J.; Cho, W.; Cha, K.-H.; Ahn, J.; Han, K.; Hwang, S.-J. Solubilization of the Poorly Water Soluble Drug, Telmisartan, Using Supercritical Anti-Solvent (SAS) Process. *Int. J. Pharm.* **2013**, *441*, 50–55. [CrossRef]
8. Isaac, J.; Ganguly, S.; Ghosh, A. Co-Milling of Telmisartan with Poly(Vinyl Alcohol)—An Alkalinizer Free Green Approach to Ensure Its Bioavailability. *Eur. J. Pharm. Biopharm.* **2016**, *101*, 43–52. [CrossRef]
9. Lepek, P.; Sawicki, W.; Wlodarski, K.; Wojnarowska, Z.; Paluch, M.; Guzik, L. Effect of Amorphization Method on Telmisartan Solubility and the Tableting Process. *Eur. J. Pharm. Biopharm.* **2013**, *83*, 114–121. [CrossRef]
10. Yu, G.; Chen, X.; He, L.; Li, X.; Zhou, Z.; Ren, Z. Study on the Solubilization of Telmisartan by Forming Cocrystals with Aromatic Carboxylic Acids. *CrystEngComm* **2021**, *23*, 4871–4878. [CrossRef]
11. Chadha, R.; Bhandari, S.; Haneef, J.; Khullar, S.; Mandal, S. Cocrystals of Telmisartan: Characterization, Structure Elucidation, in Vivo and Toxicity Studies. *CrystEngComm* **2014**, *16*, 8375–8389. [CrossRef]
12. Haneef, J.; Chadha, R. Drug-Drug Multicomponent Solid Forms: Cocrystal, Coamorphous and Eutectic of Three Poorly Soluble Antihypertensive Drugs Using Mechanochemical Approach. *AAPS PharmSciTech* **2017**, *18*, 2279–2290. [CrossRef]
13. Ganesan, T.; Muthudoss, P.; Voguri, R.S.; Ghosal, S.; Ann, E.Y.C.; Kwok, J.; Shahnawaz, S.S.; Omar, M.F.; Allada, R.; See, H.H. A New Febuxostat-Telmisartan Drug-Drug Cocrystal for Gout-Hypertension Combination Therapy. *J. Pharm. Sci.* **2022**, *111*, 3318–3326. [CrossRef]
14. Turek, M.; Różycka-Sokołowska, E.; Owsianik, K.; Bałczewski, P. New Perspectives for Antihypertensive Sartans as Components of Co-Crystals and Co-Amorphous Solids with Improved Properties and Multipurpose Activity. *Mol. Pharm.* **2024**, *21*, 18–37. [CrossRef]
15. Morissette, S.L.; Almarsson, Ö.; Peterson, M.L.; Remenar, J.F.; Read, M.J.; Lemmo, A.V.; Ellis, S.; Cima, M.J.; Gardner, C.R. High-Throughput Crystallization: Polymorphs, Salts, Co-Crystals and Solvates of Pharmaceutical Solids. *Adv. Drug Deliv. Rev.* **2004**, *56*, 275–300. [CrossRef] [PubMed]
16. Donsbach, K.; Hof, I. Crystalline Form of Telmisartan Sodium. U.S. Patent US6737432B2, 18 May 2004.
17. Zupancic, S.; Smrkolj, M.; Stropnik, T.; Vrbinc, M.; Osolnik, R.; Sedmak, G. Preparation of Telmisartan Salts. WO Patent WO2007147889A2, 12 December 2007.
18. Hatanaka, Y.; Uchiyama, H.; Kaneko, S.; Ueda, K.; Higashi, K.; Moribe, K.; Furukawa, S.; Takase, M.; Yamanaka, S.; Kadota, K.; et al. Designing a Novel Coamorphous Salt Formulation of Telmisartan with Amlodipine to Enhance Permeability and Oral Absorption. *Mol. Pharm.* **2023**, *20*, 4071–4085. [CrossRef]
19. Park, C.; Meghani, N.; Shin, Y.; Oh, E.; Park, J.-B.; Cui, J.-H.; Cao, Q.-R.; Tran, T.; Tran, P.; Lee, B.-J. Investigation of Crystallization and Salt Formation of Poorly Water-Soluble Telmisartan for Enhanced Solubility. *Pharmaceutics* **2019**, *11*, 102. [CrossRef] [PubMed]
20. Higashi, T. *ABSCOR*; Rigaku Corporation: Tokyo, Japan, 1995.
21. Rigaku Corporation. *RAPID-AUTO*; Rigaku Corporation: Tokyo, Japan, 1999.
22. Sheldrick, G.M. SHELXT—Integrated Space-Group and Crystal-Structure Determination. *Acta Crystallogr. Sect. A Found. Crystallogr.* **2015**, *71*, 3–8. [CrossRef]
23. Sheldrick, G.M. Crystal Structure Refinement with SHELXL. *Acta Crystallogr. Sect. C Struct. Chem.* **2015**, *71*, 3–8. [CrossRef] [PubMed]

24. Hübschle, C.B.; Sheldrick, G.M.; Dittrich, B. ShelXle: A Qt Graphical User Interface for SHELXL. *J. Appl. Crystallogr.* **2011**, *44*, 1281–1284. [CrossRef] [PubMed]
25. Macrae, C.F.; Sovago, I.; Cottrell, S.J.; Galek, P.T.A.; McCabe, P.; Pidcock, E.; Platings, M.; Shields, G.P.; Stevens, J.S.; Towler, M.; et al. Mercury 4.0: From Visualization to Analysis, Design and Prediction. *J. Appl. Crystallogr.* **2020**, *53*, 226–235. [CrossRef] [PubMed]
26. Mackenzie, C.F.; Spackman, P.R.; Jayatilaka, D.; Spackman, M.A. CrystalExplorer Model Energies and Energy Frameworks: Extension to Metal Coordination Compounds, Organic Salts, Solvates and Open-Shell Systems. *IUCrJ* **2017**, *4*, 575–587. [CrossRef]
27. Sanders, J. *Veusz: Scientific Plotting Package*; ASCL.net Astrophysics Source Code Library, 2023.
28. Roisnel, T.; Rodríquez-Carvajal, J. WinPLOTR: A Windows Tool for Powder Diffraction Pattern Analysis. *Mater. Sci. Forum* **2001**, *378–381*, 118–123. [CrossRef]
29. United States Pharmacopeial Convention. <1174> Powder Flow. In *United States Pharmacopeia and National Formulary (USP 44-NF 39)*; United States Pharmacopeia: North Bethesda, MD, USA, 2021.
30. United States Pharmacopeial Convention. <429> Light Diffraction Measurement of Particle Size. In *United States Pharmacopeia and National Formulary (USP 44-NF 39)*; United States Pharmacopeia: North Bethesda, MD, USA, 2021.
31. Fell, J.T.; Newton, J.M. Determination of Tablet Strength by the Diametral-Compression Test. *J. Pharm. Sci.* **1970**, *59*, 688–691. [CrossRef]
32. Dinnebier, R.E.; Sieger, P.; Nar, H.; Shankland, K.; David, W.I.F. Structural Characterization of Three Crystalline Modifications of Telmisartan by Single Crystal and High-Resolution X-ray Powder Diffraction. *J. Pharm. Sci.* **2000**, *89*, 1465–1479. [CrossRef]
33. Adrjanowicz, K.; Wojnarowska, Z.; Wlodarczyk, P.; Kaminski, K.; Paluch, M.; Mazgalski, J. Molecular Mobility in Liquid and Glassy States of Telmisartan (TEL) Studied by Broadband Dielectric Spectroscopy. *Eur. J. Pharm. Sci.* **2009**, *38*, 395–404. [CrossRef] [PubMed]
34. Saber, R.A.; Attia, A.K.; Salem, W.M. Thermal Analysis Study of Antihypertensive Drugs Telmisartan and Cilazapril. *Adv Pharm Bull* **2014**, *4*, 283–287. [CrossRef]
35. Ramos, J.J.M.; Diogo, H.P. Thermal Behavior and Molecular Mobility in the Glassy State of Three Anti-Hypertensive Pharmaceutical Ingredients. *RSC Adv.* **2017**, *7*, 10831–10840. [CrossRef]
36. Takahashi, M.; Uekusa, H. Dehydration and Rehydration Mechanisms of Pharmaceutical Crystals: Classification Of Hydrates by Activation Energy. *J. Pharm. Sci.* **2022**, *111*, 618–627. [CrossRef]
37. Jurczak, E.; Mazurek, A.H.; Szeleszczuk, Ł.; Pisklak, D.M.; Zielińska-Pisklak, M. Pharmaceutical Hydrates Analysis—Overview of Methods and Recent Advances. *Pharmaceutics* **2020**, *12*, 959. [CrossRef]
38. Spek, A.L. Structure Validation in Chemical Crystallography. *Acta Crystallogr. Sect. D Biol. Crystallogr.* **2009**, *65*, 148–155. [CrossRef]
39. Nugraha, Y.P.; Uekusa, H. Suppressed Hydration in Metoclopramide Hydrochloride by Salt Cocrystallisation. *CrystEngComm* **2018**, *20*, 2653–2662. [CrossRef]
40. United States Pharmacopeial Convention. Telmisartan Tablets. In *United States Pharmacopeia and National Formulary (USP 44-NF 39)*; United States Pharmacopeia: North Bethesda, MD, USA, 2021.
41. Guzmán, H.R.; Tawa, M.; Zhang, Z.; Ratanabanangkoon, P.; Shaw, P.; Gardner, C.R.; Chen, H.; Moreau, J.; Almarsson, Ö.; Remenar, J.F. Combined Use of Crystalline Salt Forms and Precipitation Inhibitors to Improve Oral Absorption of Celecoxib from Solid Oral Formulations. *J. Pharm. Sci.* **2007**, *96*, 2686–2702. [CrossRef]
42. Babu, N.J.; Nangia, A. Solubility Advantage of Amorphous Drugs and Pharmaceutical Cocrystals. *Cryst. Growth Des.* **2011**, *11*, 2662–2679. [CrossRef]
43. Hawley, M.; Morozowich, W. Modifying the Diffusion Layer of Soluble Salts of Poorly Soluble Basic Drugs To Improve Dissolution Performance. *Mol. Pharm.* **2010**, *7*, 1441–1449. [CrossRef]
44. Yu, L.X.; Carlin, A.S.; Amidon, G.L.; Hussain, A.S. Feasibility Studies of Utilizing Disk Intrinsic Dissolution Rate to Classify Drugs. *Int. J. Pharm.* **2004**, *270*, 221–227. [CrossRef]
45. Braun, D.E.; Koztecki, L.H.; Mcmahon, J.A.; Price, S.L.; Reutzel-Edens, S.M. Navigating the Waters of Unconventional Crystalline Hydrates. *Mol. Pharm.* **2015**, *12*, 3069–3088. [CrossRef]
46. Utama, V.K.; Soewandhi, S.N.; Nugraha, Y.P. *Intermolecular Interaction Studies of Telmisartan and Amlodipine Besylate*; Bandung Institute of Technology: Bandung, Indonesia, 2021.
47. Danjo, K.; Kinoshita, K.; Kitagawa, K.; Iida, K.; Sunada, H.; Otsuka, A. Effect of Particle Shape on the Compaction and Flow Properties of Powders. *Chem. Pharm. Bull.* **1989**, *37*, 3070–3073. [CrossRef]
48. Kudo, Y.; Yasuda, M.; Matsusaka, S. Effect of Particle Size Distribution on Flowability of Granulated Lactose. *Adv. Powder Technol.* **2020**, *31*, 121–127. [CrossRef]
49. Joiris, E.; Di Martino, P.; Berneron, C.; Guyot-Hermann, A.M.; Guyot, J.C. Compression Behavior of Orthorhombic Paracetamol. *Pharm. Res.* **1998**, *15*, 1122–1130. [CrossRef] [PubMed]
50. Wang, C.; Paul, S.; Wang, K.; Hu, S.; Sun, C.C. Relationships among Crystal Structures, Mechanical Properties, and Tableting Performance Probed Using Four Salts of Diphenhydramine. *Cryst. Growth Des.* **2017**, *17*, 6030–6040. [CrossRef]
51. Sun, C.; Grant, D.J.W. Influence of Crystal Structure on the Tableting Properties of Sulfamerazine Polymorphs. *Pharm. Res.* **2001**, *18*, 274–280. [CrossRef] [PubMed]

52. Sun, C.; Grant, D.J.W. Improved Tableting Properties of P-Hydroxybenzoic Acid by Water of Crystallization: A Molecular Insight. *Pharm. Res.* **2004**, *21*, 382–386. [CrossRef] [PubMed]
53. Chang, S.Y.; Sun, C.C. Superior Plasticity and Tabletability of Theophylline Monohydrate. *Mol. Pharm.* **2017**, *14*, 2047–2055. [CrossRef] [PubMed]
54. Sun, C.C.; Hou, H. Improving Mechanical Properties of Caffeine and Methyl Gallate Crystals by Cocrystallization. *Cryst. Growth Des.* **2008**, *8*, 1575–1579. [CrossRef]
55. Ainurofiq, A.; Mauludin, R.; Mudhakir, D.; Umeda, D.; Soewandhi, S.N.; Putra, O.D.; Yonemochi, E. Improving Mechanical Properties of Desloratadine via Multicomponent Crystal Formation. *Eur. J. Pharm. Sci.* **2018**, *111*, 65–72. [CrossRef]
56. Khomane, K.S.; More, P.K.; Raghavendra, G.; Bansal, A.K. Molecular Understanding of the Compaction Behavior of Indomethacin Polymorphs. *Mol. Pharm.* **2013**, *10*, 631–639. [CrossRef]
57. Šupuk, E.; Ghori, M.U.; Asare-Addo, K.; Laity, P.R.; Panchmatia, P.M.; Conway, B.R. The Influence of Salt Formation on Electrostatic and Compression Properties of Flurbiprofen Salts. *Int. J. Pharm.* **2013**, *458*, 118–127. [CrossRef]
58. Sun, C.C.; Kiang, Y.-H. On the Identification of Slip Planes in Organic Crystals Based on Attachment Energy Calculation. *J. Pharm. Sci.* **2008**, *97*, 3456–3461. [CrossRef] [PubMed]
59. Keshavarz, L.; Pishnamazi, M.; Rao Khandavilli, U.B.; Shirazian, S.; Collins, M.N.; Walker, G.M.; Frawley, P.J. Tailoring Crystal Size Distributions for Product Performance, Compaction of Paracetamol. *Arab. J. Chem.* **2021**, *14*, 103089. [CrossRef]
60. Wang, Z.; Solomos, M.; Axnanda, S.; Chen, C.; Figus, M.; Schenck, L.; Sun, C.C. Varied Bulk Powder Properties of Micro-Sized API within Size Specifications as a Result of Particle Engineering Methods. *Pharmaceutics* **2022**, *14*, 1901. [CrossRef] [PubMed]
61. Sun, C.C.; Himmelspach, M.W. Reduced Tabletability of Roller Compacted Granules as a Result of Granule Size Enlargement. *J. Pharm. Sci.* **2006**, *95*, 200–206. [CrossRef] [PubMed]